Nano-Scale Synthesis of the Complex Silicate Minerals Forsterite and Enstatite

Lawrence M. Anovitz[1*]

Adam J. Rondinone[2]

Lindsay Sochalski-Kolbus[3]

Jörgen Rosenqvist[1,4]

Michael C. Cheshire[1]

For submission to

Journal of Colloid and Interface Science

Draft of Dec 22, 2016

[1] Chemical Sciences Division, MS 6110, P.O. Box 2008, Bldg. 4100, Oak Ridge National Laboratory, Oak Ridge, Tennessee 37831-6110

[2] Center for Nanophase Materials Science Division, MS 6494, P.O. Box 2008, Bldg. 8610, Oak Ridge National Laboratory, Oak Ridge, Tennessee 37831-6494

[3] Chemical and Engineering Materials Division, MS 6454, P.O. Box 2008, Bldg. 8600, Oak Ridge National Laboratory, Oak Ridge, Tennessee 37831-6454

[4] Present address: Department of Chemistry and Molecular Biology University of Gothenburg SE-412 96 Gothenburg Sweden

Abstract

Olivine is a relatively common family of silicate minerals in many terrestrial and extraterrestrial environments, and is also useful as a refractory ceramic. A capability to synthesize fine particles of olivine will enable additional studies on surface reactivity under geologically relevant conditions. This paper presents a method for the synthesis of nanocrystalline samples of the magnesium end-member, forsterite (Mg_2SiO_4) in relatively large batches (15-20 grams) using a sol-gel/surfactant approach. Magnesium methoxide and tetraethylorthosilicate (TEOS) are refluxed in a toluene/methanol mixture using dodecylamine as a surfactant and tert-butyl amine and water as hydrolysis agents. This material is then cleaned and dried, and fired at 800°C. Post-firing reaction in hydrogen peroxide was used to remove residual organic surfactant. X-ray diffraction showed that a pure material resulted, with a BET surface area of up to 76.6 m^2/g. The results of a preliminary attempt to use this approach to synthesize nano-scale orthopyroxene ($MgSiO_3$) are also reported.

1. Introduction

Olivine, $(Mg,Fe,Mn,Ca)_2SiO_4$, is a family of orthosilicate minerals with a relatively simple structure (silicate tetrahedra linked to magnesium octahedra through oxygen bonds). It is one of the most abundant minerals in the Earth, comprising much of the mantle and oceanic crust, and is also abundant in many terrestrial environments, such as the Columbia River basalts and the New York Palisades. It is also common in extraterrestrial environments such as the surface and mantle of the Moon and Mars, asteroids (e.g. Vesta), and a variety of other extraterrestrial materials such as meteorites and interplanetary dust particles (IDPs)[1-3]. In addition, its refractory nature and insulating properties make it a useful ceramic material as well[4].

While less abundant, pyroxenes also play an important role in many geological and extraterrestrial environments. For example, the presence of clino- and orthopyroxenes in metamorphosed mafic rocks defines the granulite facies[5-7], they are common components in a wide variety of igneous rocks[8], and pigeonites were found to be important components of lunar samples[9]. Pyroxene compositions have also been used for the fabrication of glass-ceramics[10-13], and phosphors[14]. The pyroxene structure is more polymerized than that of the olivines, as it is a single-chain silicate with two octahedral sites located between the chains. While the range of solid-solutions defined by potential and known end-member phases is much larger in the pyroxenes than in olivines, the enstatite ($MgSiO_3$) – ferrosilite ($FeSiO_3$) join is compositionally analogous to that of the common olivine join forsterite (Mg_2SiO_4) – fayalite (Fe_2SiO_4).

Recently the potential significance of forsterite (and pyroxene) for our understanding of Earth's history has increased significantly with the publication of a theory[15-18] that proposed that water incorporation occurred by means of adsorption of water on dust particles, beginning at stage one of planet formation when dust and water gas were still present in the accretion disk.

Astronomical observations show that dust clouds consist of Mg-rich olivine (Mg_2SiO_4, forsterite), pyroxenes and other refractory minerals with radii <1 μm^2. Several authors[19-21] suggest that these refractory minerals should coalesce during stage 1 of planet formation by means of low-velocity impacts creating low-density, irregularly shaped fractal structures. Stimpfl et al.[16-18] suggested that the concomitant presence of small fractal particulates with high surface area and water gas in an environment of low-energy impacts could lead to adsorption of 1 and 3 times the volume of the Earth's oceans onto the dust that eventually accreted to form our planet.

The influence of water in geochemical processes under nearly all conditions has been, and remains, one of the most important issues in geochemistry. Water is the ultimate arbiter of weathering, and plays an important role in metamorphic and igneous processes as well. Water species are ubiquitous on the surfaces of metal oxides in humid environments, and may adsorb almost instantaneously on silica even at high vacuum[22]. Studies of the surface chemistry of oxides, especially rutile and cassiterite, show that water may chemisorb either associatively or dissociatively (as H_2O or OH^-), and physisorption processes often involve close interactions of water with the surface in several layers of different structures, whose properties trend towards those of bulk water with increasing distance from the surface[23-27].

In order to experimentally analyze the sorption of water on solids, however, a key factor is the availability of starting materials with large surface areas. This is especially true for neutron spectroscopic approaches such as quasi-elastic and inelastic neutron scattering[24,25,27-30], in which the relatively low fluxes of even the best sources tend to necessitate the use of large samples. Nanoparticulate materials also provide the opportunity to more easily study the surface energies of the materials involved through titration[31-34] and calorimetric analyses[4,35-36]. Several studies have investigated the use of forsterite as a starting material for geological carbon sequestration

by reaction of forsterite with CO_2 to form magnesite ($MgCO_3$)[37-49]. Forsterite has also been suggested as a possible drug delivery route and for use in other medical applications[50-54].

In order to facilitate the study of the surface properties of olivines and pyroxenes, and the nature of their surface interactions with water and CO_2, a method is, therefore, needed to synthesize nano-scale end-member forsterite and enstatite with sufficiently large surface areas, and in sufficiently large quantities (10's of grams) to permit such measurements to be made. This paper outlines a successful method designed to synthesize nano-scale olivine, and a preliminary attempt to use a slight modification of this method to synthesize nano-scale enstatite as well.

2. Previous Work

Several methods for synthesis of micro or nanoforsterite and/or enstatite have been reported in the literature[4,53-81]. With the exception of[58,63,69-71] these focused on synthesis of forsterite. Several, however, yielded impure results. Douy[71] noted that, of the older works he evaluated[55-59,65,67,69,70] "only Burlitch et al.[57] succeeded in preventing the phase separation of MgO". This was also true of others[66,75,76], and purposely so of the results of McDonnell et al.[72]. Unfortunately, the approach of Burlitch et al.[57], which worked for both forsterite and an intermediate forsterite/fayalite solid solution (Fo_{90}), generated relatively coarse particles (approx. 5 – 10 μm) once the powder was crystallized. The approach of Hassanzadeh-Tabrizi et al.[53] yielded high surface area, mesoporous rod-like structures.

One goal of our project was to synthesize nanoforsterite/enstatite using a relatively simple approach to yield relatively equant crystal forms. Thus, we avoided those techniques that required specialized equipment or aimed at specific crystal shapes. The first method of Douy[71], for instance, requires a spray drier, and generates relatively coarse particles and aggregates.

Similarly, the method of Tani et al.[76] requires a spray flame reactor, while the method of Tsai[73] was primarily aimed at creating fibers. The approaches of Kosanovic et al., Chen et al., Mirhadi et al., and Barzegar Bafrooei et al.[54,74,80,81] require high-energy ball milling and, for Kosanovic et al.[73], because one of the starting materials is NH_4-exchanged Zeolite A, which is aluminous, cannot yield a pure result. The second approach of Douy[71] required very high firing temperatures, which resulted in slight Mg losses from the forsterite structure. As could be expected, changes in firing temperature also led to changes in the enstatite polymorph formed.

Of the purely chemical, largely sol-gel, approaches Chen and Navrotsky[4] followed a sucrose template approach[77] and obtained a maximum surface area of 31.32 m^2/g (BET), which is yet larger than the value reported by Saberi et al.[77] using a citrate/nitrate method (14.95 m^2/g). The particles obtained by Chen and Navrotsky[4] also appear to be less agglomerated than those of Saberi et al.[77,78]. Ni et al.[75] was focused on generating relatively coarsely crystalline bioceramics, and the intermediate powders were highly aggregated. Sanosh et al.[79] used a simple method, aging and then calcining a sol-gel formed from magnesium nitrate hexahydrate and tetraethylorthosilicate (TEOS). This yielded fine particles, but the results appeared to be agglomerated, and no surface areas are given.

Many of these techniques also used magnesium nitrate hexahydrate as a starting material. This has the disadvantage that a hydrated starting material is more likely to prematurely hydrolyze TEOS before atomic-level mixing TEOS and nitrate salts can occur. By contrast, our approach is mostly anhydrous, which is expected to yield better mixing at the atomic level and a controlled hydrolysis thereafter. Park et al.[60-62] successfully used a sol-gel method (based on the approach of Burlitch et al.[57]) using magnesium or magnesium methoxide ($Mg(OMe)_2$) and TEOS starting materials as well as an approach using poly(methacrylate) precursors. They found that

the addition of water to the atmosphere used to calcine the resultant powders, and the presence of residual carbon, aided in formation of pure forsterite. While the results of the poly(methacrylate) approach were somewhat impure, the sol-gel yielded pure forsterite. No surfactants were used in the sol-gel syntheses, although a strong base $(Bu^n)_4NOH$ was added to help complete hydrolysis, but the resulting surface area was relatively small (< 4.5 m^2/g)

From the above discussion, and as noted by Douy[71], it is clear that the synthesis of pure, high surface area nanoforsterite and, by extension, nanoenstatite, is difficult. It is, therefore, apparent that a relatively simple method yielding single-phase, high surface area forsterite that can also be used to synthesize enstatite and other pyroxenes is needed. As the approach of Burlitch et al.[57] and Park et al.[60-62] yielded a pure material using a relatively simple approach, we have modified it to generate non-agglomerated, high surface area materials.

3. Synthesis and Characterization of Nanoforsterite and Nanoenstatite

2.1 Starting materials

Starting materials for this synthesis consisted of methanol (Fisher Scientific), toluene (Fisher Scientific), magnesium methoxide (Alfa Aesar), tetraethylorthosilicate, TEOS, (Acros Organics), dodecylamine (Aldrich), and tert-butyl amine (Aldrich). These were used as received. Deionized (DI) water was generated by a Millipore water purification system, and had a resistivity of at least 18 MΩ•cm.

2.2 Synthesis Method

Synthesis was begun by attaching a glass condenser to a 1-liter, 3 neck flask. The top of the condenser was attached to a Schlenk line, and the flask was placed in a silicone oil bath on a

magnetic stirrer/hotplate. A recirculating bath set at 18°C was attached to the condenser. A stirbar was added to the flask, and the flask and condenser were evacuated for several hours. The flask was then backfilled with Ar, which was allowed to continue flowing. 375 mL of toluene and 175 ml of methanol were then added and allowed to stir for a few minutes to homogenize the solution.

The magnesium component of the synthesis was obtained from a magnesium methoxide ($Mg(OMe)_2$) solution. This was analyzed by hydrolyzing approximately 1 gram of the solution with concentrated HCl, then drying the resultant solution and firing in air at 800°C overnight. Comparison of the weight of the resultant MgO powder with the initial weight of magnesium methoxide provided the concentration of MgO in the solution, which ranged from 4.3 to 4.5 weight percent. A portion of the magnesium methoxide solution was then transferred to a 1 L Nalgene bottle for easier handling. This was backfilled with Ar and sealed when not in use to keep the solution from reacting with atmospheric water. Silica was obtained using tetraethylorthosilicate (TEOS). A similar approach was used to test its composition, which was found to closely approximate the theoretical value.

For each forsterite synthesis run, the goal was to add approximately 175 g of magnesium methoxide to the solvent mixture. Half of that amount was added for enstatite. To do so, a vertical cm scale was marked on the Nalgene bottle. The bottle was weighed, approximately 3.5 cm of solution poured into the three-neck flask with Ar running to limit air access, and then the bottle was refilled with Ar, closed and reweighed. This provided the mass of magnesium methoxide used, and an estimate of solution density for use in future syntheses. The solvent solution was then allowed to stir for 5 minutes, followed by addition of a stoichiometric mass of TEOS calculated from the mass of magnesium methoxide actually used. The resultant solution

was then allowed to stir again for at least 5 minutes while amine solution was prepared for use as a surfactant/hydrolysis agent.

The amine solution was prepared by first adding 8.75 g melted dodecylamine, the surfactant used in this process, to 50 mL of toluene. To this was then added 1.75 g of tert-butylamine, the hydrolysis agent. The resultant solution was added last to the 3-neck flask, and the whole was then stirred again for 5 minutes. At this point the cooling water for the condenser was turned on, and the hot plate heated to 250°C, bringing the solvent mixture to reflux temperature in 20-30 minutes. Within 5-10 minutes of reflux being achieved the solution turned cloudy, indicating the formation of (nano)particles. The solution was allowed to heat for at least 1 hour, after which the Ar flow was turned off, and ~2 ml of water were added, dropwise, to the mixture, turning it a milkier white. This was done to assure that the hydrolysis was as complete as possible. The solution was then allowed to reflux overnight, two additional ~2 ml water additions were made the next morning and early afternoon, and the heat was turned off in the evening, typically ~ 24-26 hours after heating was begun.

Once the solution cooled it was spun down in an Eppendorf multipurpose centrifuge at 9000 rpm for 15 minutes. The solvent was decanted and discarded, leaving the gel in the centrifuge tubes. These were then refilled with a 2:1 mixture of toluene and methanol, and the gel re-suspended using an ultrasonic probe followed by a Vortex mixer. The re-suspended gel was then again spun down and the new solvent again decanted and discarded. This step was repeated three times in order to remove as much as possible of the surplus amine. The remaining gel was then dried in air, ground, and fired (2 hours to 800°C, 2 hours at 800°C, cool in place in the furnace). This firing crystallized the initially amorphous nanoparticles. Once the sample had cooled, it was ground in an agate shatterbox and any remaining organic material was removed by

immersing the sample in a 30 % H_2O_2 solution until reaction stopped to remove any remaining organic material. X-ray diffraction of the samples after peroxide treatment showed that they remained forsterite/enstatite.

2.3 Characterization Methods

The phases present in each synthesis run were identified by powder x-ray diffraction (XRD) using a Panalytical Empyrean diffractometer with CuK$\alpha_{1,2}$ incident radiation (z = 1.54 Å) operated at 45 keV and 40 mA. The XRD data were collected at room temperature using powder dispersed on a zero-background silicon plate. Data were collected between 10 and 120 degrees 2Θ, with a step size of 0.016° and a count time of 325 seconds per step, ¼ mm incident and diffracted beam slits, and a ½ mm anti-scatter slit. A diffracted beam monochromator and a nickel filter were used to remove fluorescence and Kβ radiation, and the patterns were examined using High Score Plus[82] for Rietveld refinement. The diffraction pattern and specific surface area of each sample was obtained both before and after H_2O_2 treatment. The specific surface area was obtained using a Quantachrome Autosorb 1 Brunauer-Emmett-Teller (BET) analyzer at liquid nitrogen temperatures. Nitrogen was used as the absorbant. In addition, an example of each of the synthetic powders was imaged using a Zeiss Libra 120Plus transmission electron microscope and a Hitachi S-4800 scanning electron microscope. Samples for TEM were collected before the powders were treated with H_2O_2. Samples for SEM analysis were carbon coated and imaged at 15 kV.

3.0 Results and Discussion

3.1 X-Ray Diffraction

Figures 1 and 2 shows typical XRD patterns for forsterite and enstatite grown in the manner described above. As can be seen, both are well crystallized. For forsterite, no other phases are present at the detection level of the scan (probably < 1mole percent). Rietveld refinement of the forsterite pattern yielded unit cell parameters: a = 10.1993(3) Å, b = 5.9763(1) Å, and c = 4.7467(1) Å in the orthorhombic space group Pnma, with an R value of 6.15%. In the case of enstatite both ortho- and clino- enstatite were present, as was a small percentage of forsterite. Refinement of the enstatite pattern yielded a = 9.131(2) Å, b = 8.800(2) Å, and c = 5.261(2) Å with and R value of 7.48 in orthorhombic space group Pbcn for orthoenstatite, a = 9.349(5) Å, b = 8.797(4) Å, and c = 5.192 Å, β = 102.70(4)° in monoclinic space group $P2_1/c$, with and R value of 8.55% for clinoenstatite, and a = 9.865(3) Å, b = 6.148(2) Å, and c = 4.763(2) Å with an R value of 13.31 in orthorhombic space group Pnma for forsterite.

This polymorphic assemblage has been a problem in previous attempts to synthesize nano-enstatite. Echeverría[58] generated unagglomerated, 300-600 Å, approximately spherical particles, with a surface area of 108 m^2/g, which were then densified into an interlocking mosaic of 0.5 μm grains of ortho-, clino- and protoenstatite. Hayashi et al.[63] appear to have formed clinoenstatite, but only a single X-ray peak was reported, so it is uncertain if any of the other polymorphs were present. Jones et al.[70] also obtained either mixtures or pure protoenstatite. Ban et al.[69] do appear to have made orthoenstatite from TEOS (or tetramethyoxysilane), water and magnesium metal in methanol starting materials at 700°C, but no information on the particle size or surface area was provided. The experiments of Douy[71] formed all three polymorphs, although

they were able to convert the material to nearly pure protoenstatite on firing at 1500°C for one hour. This fact that a mixture of enstatite polymorphs was formed in our experiment as well suggests that a refinement of the method is needed for enstatite if pure ortho- or clino-nano-enstatite (high or low) are to be created. This may include addition of extra TEOS, and/or a change in firing temperature or time. Although the temperature of the experiment (800°C) is already significantly above the accepted equilibrium transition temperature of 566°C at 1 bar, the transformation is known to be quite slow[83-85], and similar forsterite and crystobalite impurities were noted by Turnock et al.[85], who heated their materials at up to 1200°C. Significantly higher temperatures, however, risks the formation of protoenstatite, which becomes stable about 985 ±10 °C[86]. Care would also have to be taken in such a case to avoid unwanted growth of the nanoparticles.

3.2 BET

The white color of the material after triple washing and subsequent firing suggested that the multiple washing steps had removed the organic components from the amines (failure to triple-wash the sample prior to drying and firing yielded a dark grey product). For forsterite, however, comparison of BET results before and after the hydrogen peroxide treatment suggested that this was not the case. BET analyses of the initially synthesized material yielded surface areas ranging from 16.9 to 24.6 m^2/g, respectively. After peroxide treatment, however, surface areas ranged from 38.9 to 76.7 m^2/g. For enstatite, however, the opposite effect was observed. The as-synthesized material had a surface area of 13.0 m^2/g, but after hydrogen peroxide treatment this dropped to 9.3 m^2/g. The origin of this loss is uncertain, but it may reflect the relative tendencies of the materials to aggregate when dry, artificially reducing the surface area measured by BET,

initial surface area formed by the organic contaminants, or possible reaction of the enstatite with the peroxide.

3.3 SEM/TEM

Figure 3 shows an energy dispersive X-ray spectrum of one of the samples of synthetic forsterite. As expected, only magnesium, silicon and oxygen are present (minor carbon and aluminum peaks are artifacts from the sample mount, which was carbon tape on an aluminum plate. Figures 4-5 show SEM and TEM images of the synthetic forsterite. The forsterite images are from the sample that had the largest surface area analyzed – 76.7 m^2/gm. Although the measured specific surface areas given above (section 3.2) suggest the average particle diameter should be in the range of 25 to 45 nm (calculated assuming uniform particle size and spherical particles) it is clear from the SEM data that many of the particles are agglomerated into ball-like structures that are themselves agglomerated into larger particles. The grain shown in the TEM image is also relatively large, but may show the preliminary formation of crystal faces that are not apparent in the SEM.

Figure 6 shows an energy dispersive X-ray spectrum of one of the samples of synthetic enstatite. Again, only magnesium, silicon and oxygen are present except for minor carbon and aluminum peaks, which are artifacts from the sample mount. SEM and TEM images of the synthetic enstatite sample is shown in Figures 7 and 8. As with the forsterite, the enstatite particles are approximately spherical and appear to be agglomerations of smaller particles. Those shown in the SEM images vary from ~50 to 400 nm, while the particle shown in the TEM image has a diameter of approximately 40 nm. The measured specific surface areas suggest diameters in the range 140 to 200 nm, which is consistent with these observations. In both cases the

samples had not been treated with hydrogen peroxide, and small amounts of organic matter appear to still be present, despite the high temperatures at which the samples were fired. This is consistent with the observation that the samples reacted for various periods of time when treated with H_2O_2.

4. Conclusions

As can be seen from the above results, the approach developed here has been very successful in providing significant quantities of high surface area forsterite and enstatite. Typical forsterite and enstatite runs using a 1-liter three-necked flask yielded 15 to 20 grams of well-crystallized material per run. Importantly, to the extent we could ascertain the material resulting from this approach is quite pure. No secondary phases were identified by XRD, or seen in TEM for the forsterite if the stoichiometry of the starting material was maintained and the organics were removed. Some refinement of the method, probably in terms of firing temperature or time, does appear to be needed for enstatite, however, to obtain pure polymorphs. As noted in the descriptions of other approaches above, both are significant advantages of the technique described. This material will, therefore, allow reasonably simple synthesis of high surface area forsterite for several applications, including analysis of surface dynamics, thermodynamics and absorption of fluids such as those proposed as crucial to the initial acquisition of the earth's water[15-18], reaction kinetics for potential carbon sequestration applications, medical applications such as drug delivery systems, and synthesis of refractory ceramics. The agglomerated appearance of the forsterite, however, suggests that even greater surface areas may be achieved, possibly by grinding the material prior to firing. The success of this approach for synthesis of both forsterite and enstatite suggests that it may be modified to yield other olivines and

pyroxenes, and perhaps other silicates as well. A similar approach may also be useful for making germinate analogues[87].

AUTHOR INFORMATION

Corresponding Author

*anovitzlm@ornl.gov

Chemical Sciences Division

One Bethel Valley Rd., P.O. Box 2008 MS 6110

Oak Ridge National Laboratory, Oak Ridge TN, USA, 37831-6110

Author Contributions

The manuscript was written through contributions of all authors. All authors have given approval to the final version of the manuscript. LMA and AJR conceived of the experiment while LMA, AJR, LMSK, and JR carried out the experiment, MCC obtained the SEM images and EDA spectrum.

5. Acknowledgements

Effort by LMA, LMSK, JR and MCC was supported by research sponsored by the Division of Chemical Sciences, Geosciences, and Biosciences, Office of Basic Energy Sciences, U.S. Department of Energy. The synthesis of the forsterite and TEM imaging of all samples was conducted at the Center for Nanophase Materials Sciences, which is a DOE Office of Science User Facility.

6. References

[1] D.S. Brownlee, Ann. Rev. Earth Planet. Sci. 13 (1985) 147.

[2] R. van Boekel, M. Min, Ch. Leinert, L.B.F.M. Waters, A. Richichi, O. Chesneau, C. Dominik, W. Jaffe, A. Dutrey, U. Graser, Th. Henning, J. de Jong, R. Köhler, A. de Koter, B. Lopez, F. Malbet, S. Morel, F. Paresce, G. Perrin, Th. Preibisch, F. Przygodda, M. Schoöller, M. Wittkowski, Nature 432 (2004) 479.

[3] T. Nakamura, T. Noguchi, T. Yada, Y. Nakamuta, N. Takaoka, Geochim. Cosmochim. Acta 65 (2001) 4385.

[4] S. Chen, A. Navrotsky, Amer. Mineral. 95 (2010) 112.

[5] H.G.F. Winkler Petrogenesis of Metamorphic Rocks, 5th ed. Springer Verlag, New York, 1979. 348 pp.

[6] F.J. Turner, Metamorphic Petrology: Mineralogical, Field, and Tectonic Aspects, 2nd Ed. McGraw Hill, New York, 1981. 524 pp.

[7] F.S. Spear, Metamorphic Phase Equilibria and Pressure-Temperature-Time Paths, 2nd Ed.. Mineral. Soc. Am .Monograph, 1994. 799 pp.

[8] P. Robinson, P. Reviews in Mineralogy 7 (1980) 419.

[9] J.J. Papike, Reviews in Mineralogy 7 (1980) 495.

[10] S.N. Salama, E.A. Saad, H. Darwish, H.A. Abo-Mosallam, Ceramics International 31 (2005) 559.

[11] F.J. Torres, J. Alarcón, Ceramics International 31 (2005) 683.

[12] A.A. Abdurakhmanov, Sh.A. Faiziev, R. Yu. Akbarov, S. Kh Suleimanov, M. Kh Rumi, M.S. Paizullakhanov, E.Z. Nodirmatov, Applied Solar Energy 45 (2009) 45.

[13] Sh.A Faiziev, M.S. Paiullakhanov, S.S. Mukhsimov, Applied Solar Energy 46 (2010) 301.

[14] Z. Xia, Y. Zhang, M.S. Molokeev, V.V Atuchin, Y. Luo, Scientific Reports 3, (2013) 3310.

[15] M.J. Drake, Meteoritics and Planetary Science 40 (2005) 519.

[16] M. Stimpfl D.S. Lauretta, M.J. Drake, Meteoritics and Planetary Science 39 (2004) A99.

[17] M. Stimpfl, M.J. Drake, N.H. de Leeuw, P. Deymier, A.M. Walker, Geochimica et Cosmochimica Acta 70 (2006) A615.

[18] M. Stimpfl, A.M. Walker, M.J. Drake, N.H. de Leeuw, P. Deymier, Journal of Crystal Growth 294 (2006) 83.

[19] S.J. Weidenschilling, J.N. Cuzzi, (1999) Protostar and Planets, vol. III, University of Arizona Press, Tucson, London, 1999.

[20] J. Blum, G. Wurm, Icarus 143 (2000) 138.

[21] M. Fogel, C.M. Leung, Astrophys. J. 501 (1998) 175.

[22] R.K. Iler, The Chemistry of Silica. John Wiley and Sons, New York, 1979. 866 pp.

[23] L. Vlcek, Z. Zhang, M.L. Machesky, P. Fenter, J. Rosenqvist, D.J Wesolowski, L.M. Anovitz, M. Predota, P.T. Cummings, Langmuir 23 (2007) 4925.

[24] E. Mamontov, L. Vlcek, D.J. Wesolowski, P.T. Cummings, W. Wang, L.M. Anovitz, J. Rosenqvist, C.M. Brown, V.G. Sakai, J. Phys. Chem. C 111 (2007) 4328.

[25] E. Mamontov, L. Vlcek, D.J. Wesolowski, P.T. Cummings, J. Rosenqvist, W. Wang, D.R. Cole, L.M. Anovitz, G. Gasparovic, Phys. Rev. E 79 (2009) 051504.

[26] D.J. Wesolowski, J.O. Sofo, A.V. Bandura, Z. Zhang, E. Mamontov, M. Predota, N. Kumar, J.D. Kubicki, P.R.C. Kent, L. Vlcek, M.L. Machesky, P.A. Fenter, P.T. Cummings, L.M. Anovitz, A.A. Skelton, J. Rosenqvist, J. Phys. Rev. B 85 (2012) 167401.

[27] H.W. Wang, D.J. Wesolowski, T.E. Proffen, L. Vlcek, W. Wang, L.F. Allard, A.I.

Kolesnikov, M. Feygenson, L.M. Anovitz, R.L. Paul, J. Amer. Chem. Soc. 135 (2013) 6885.
[28] E. Mamontov, J. Chem. Phys. 121 (2004) 9087.
[29] E. Mamontov, J. Chem. Phys. 123 (2005a) 024706.
[30] E. Mamontov, J. Chem. Phys. 123 (2005b) 171101.
[31] D.J. Wesolowski, M.L. Machesky, D.A. Palmer, L.M. Anovitz, Chemical Geology 167 (2000) 193.
[32] T. Otake, D.J. Wesolowski, L.M. Anovitz, L.F. Allard, H. Ohmoto, Earth Plan. Sci. Lett. 257 (2007) 60.
[33] D.A. Palmer, M.L. Machesky, P. Benezeth, D.J. Wesolowski, L.M. Anovitz, J.C. Deshon, J. Solution Chem. 38 (2009) 907.
[34] J. Rosenqvist, M.L. Machesky, L. Vlcek, P.T. Cummings, D.J. Wesolowski, Langmuir 25 (2009) 10852.
[35] A. Navrotsky, L. Mazeina, J. Majzlan, Science 319 (2008) 1635.
[36] A. Navrotsky, Chem. Phys. Chem. 12 (2011) 2207.
[37] KS Lackner, Ann. Rev. Energy and the Environment 27 (2002) 193.
[38] KS Lackner, CH Wendt, DP Butt, EL Joyce Jr, DH Sharp, Energy 20 (1995) 1153.
[39] EH Oelkers, DR Cole, Elements 4 (2008) 305.
[40] EH Oelkers, SR Gislason, J Matter, Elements 4 (2008) 333.
[41] JS Loring, CJ Thompson, ZM Wang, AG Joly, DS Sklarew, HT Schaef, ES Ilton, KM Rosso, AR Felmy, Environ. Sci. Technol. 2011, 45, 6204.
[42] JH Kwak, JZ Hu, RVF Turcu, KM Rosso, ES Ilton, CM Wang, JA Sears, MH Engelhard, AR Felmy, DW Hoyt, Int. J. Greenhouse Gas Control 2011, 5, 1081.
[43] JG Blencoe, DA Palmer, LM Anovitz, JS Beard US Patent 20,040,213,705 (2012).
[44] S Kerisit, JH Weare, AR Felmy, Geochim. Cosmochim. Acta 84 (2012) 137.
[45] AR Felmy, O Qafoku, BW Arey, JZ Hu, M Hu, HT Schaef, ES Ilton, NJ Hess, CI Pearce, J Feng, KM Rosso, Geochim. Cosmochim. Acta 91 (2012) 271.
[46] HT Schaef, BP McGrail, JL Loring, ME Bowden, BW Arey, KM Rosso, Environ. Sci. Technol. 47 (2013) 174.
[47] CJ Thompson, JS Loring, KM Rosso, ZM Wang, Int. J. Greenhouse Gas Control 18 (2013) 246.
[48] O Qafoku, JZ Hu, NJ Hess, MY Hu, ES Ilton, J Feng, BW Arey, AR Felmy, Geochim. Cosmochim. Acta 134 (2014) 197.
[49] JS Loring, J Chen, P Bénézeth, O Qafoku, ES Ilton, NM Washton, CJ Thompson, PR Martin, BP McGrail, KM Rosso, AR Felmy, HT Schaef, Langmuir 31 (2015) 7533.
[50] M. Kharaziha, M.H. Fathi, Ceram. Int. 35 (2009) 2449.
[51] M. Kharaziha, M.H. Fathi, J. Mech. Behav. Biomed. 3 (2010) 530.
[52] S. Ramesh, A. Yaghoubi, K.Y.S. Lee, K.M.C. Chin, J. Purbolaksono, M. Hamdi, M.A. Hassan, J. Mech. Behav. Biomed. 25 (2013) 63.
[53] SA Hassanzadeh-Tabrizi, A Bigham, M Rafienia, Materials Science and Engineering C 58 (2016) 737.
[54] SM Mirhadi, A Forghani, F Tavangarian, Ceramics International 42 (2016) 7974.
[55] N.P. Bansal, J Am Cerain Soc. 71 (1988) 666.
[56] A. Kazakos, S. Komarneni, R. Roy, Materials Letters 9 (1990) 405.
[57] J.M. Burlitch, M.L. Beeman, B. Roiley, D.L. Kojlstedt, Chem. Mater. 3 (1991) 692.
[58] L.M. Echeverría, Journal of Non-Crystalline Solids 147-148 (1992) 559.

[59] M.H.E. Martin, C.K. Ober, C.R. Hubbard, W.D. Porter, O.B. Cavin, Journal of the American Ceramic Society 75 (1992) 1831.
[60] D.G. Park, J.M. Burlitch, R.F. Geray, R. Dieckmann, D.B. Barber, C.R. Pollock, Chemistry of Materials 5 (1993) 518.
[61] D.G. Park, M.H.F. Martin, C.K. Ober, J.M. Burlitch, O.B. Cavin, W.D. Porter, C.R. Hubbard, Journal of the American Ceramic Society 77 (1994a) 33.
[62] D.G. Park, J.C. Duchamp, T.M. Duncan, J.M. Burlitch, Chemistry of Materials 6 (1994b) 1990.
[63] S. Hayashi, K.-I. Ishizu, S. Kikuchi, K. Okada, N.J. Otsuka, Europ. Ceram. Soc. 15 (1995) 521.
[64] N.I. Maliavski, O.V. Dushkin, J.V. Markina, G, Scarinci, Aiche Journal 43 (1997) 2832.
[65] M.B.D. Mitchell, D. Jackson, P.F. James, Journal of Sol-Gel Science and Technology 13 (1998a) 359.
[66] M.B.D. Mitchell, D. Jackson, P.F. James, Journal of Non-Crystalline Solids 225 (1998b) 125.
[67] M.B.D. Mitchell, D. Jackson, P.F. James, Journal of Sol-Gel Science and Technology 15 (1999) 211.
[68] M.B.D. Mitchell, D. Jackson, P.F. James, Journal of Sol-Gel Science and Technology 26 (2003) 777.
[69] T. Ban, Y, Ohya, Y.J. Takahashi, J. Am. Ceram. Soc. 82 (1999) 22.
[70] S.A. Jones, S. Wong, J.M. Burlitch, Chem. Mater. 9 (1997) 2567.
[71] A. Douy, Journal of Sol-Gel Science and Technology 24 (2002) 221.
[72] R.D. McDonnell, C.J. Spiers, C. J. Peach, J. Physics and Chemistry of Minerals 29 (2002) 19.
[73] M.T. Tsai, Materials Research Bulletin 37 (2002) 2213.
[74] C. Kosanović, N. Stubičar, N. Tomašić, V. Bermanec, M. Stubičar, Journal of Alloys and Compounds 389 (2005) 306–9.
[75] S. Ni, L. Chou, J. Chang, Ceramics International 33 (2007) 83.
[76] T. Tani, S. Saeki, T. Suzuki, Y. Ohishi, Journal of the American Ceramic Society 90 (2007) 805.
[77] A. Saberi, B. Alinejad, Z. Negahdari, F. Kazemi, A. Almasi, Materials Research Bulletin 42 (2007) 666-673.
[78] A. Saberi, Z. Negahdari, B. Alinejad, F. Golestani-Fard, Ceramics International 35 (2009) 1705.
[79] K.P. Sanosh, A. Balakrishnan, L. Francis, T.N. Kim, Journal of Alloys and Compounds 495 (2010) 113.
[80] H Barzegar Bafrooei, T Ebadzadeh, H Majidian Ceramics International 40 (2014) 2869.
[81] L Chen, G Ye, W Zhou, J Dijkmans, B Sels, A Malfliet, M Guo, Ceramics International 41 (2015) 12651.
[82] High Score Plus (2009). High Score Plus, version 3.0 (computer software), PANalytical B.V., Amelo, The Netherlands.
[83] J.E. Grover, Eos Trans AGU 53 (1972a) 539.
[84] J.E. Grover, Two problems in pyroxene mineralogy. PhD thesis, Yale University, New Haven, 1972b, 197 pp.
[85] A.C. Turnock, D.H. Lindsley, J.E. Grover, Amer. Mineral. 50 (1973) 50.

[86] T. Gasparick, Phase Diagrams for Geoscientists: An Atlas of the Earth 's Interior. Springer, 2014. 462 pp.
[87] A Navrotsky, J. Amer. Ceram. Soc 53 (1970) 696.

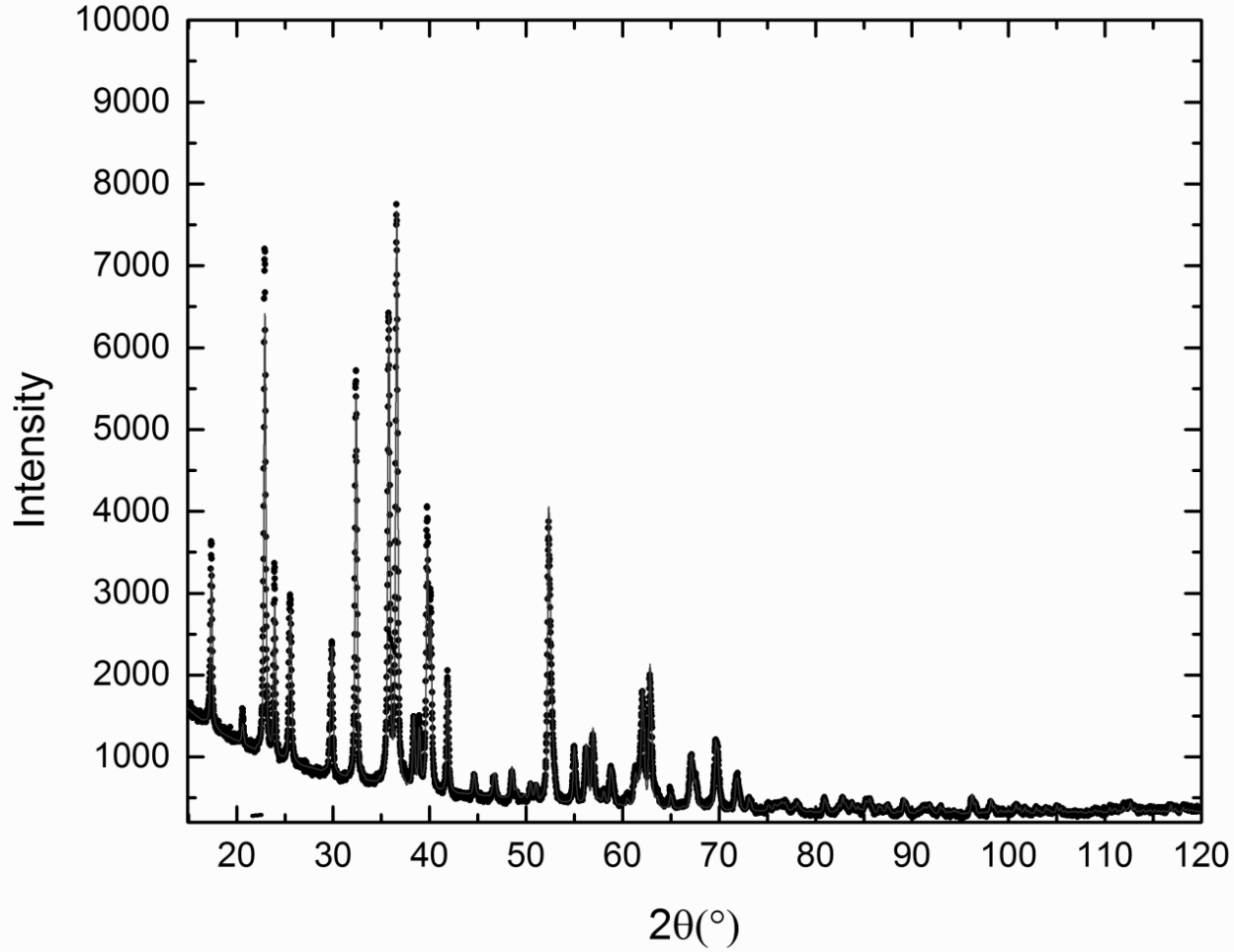

Figure 1: X-ray diffraction pattern for synthetic forsterite.

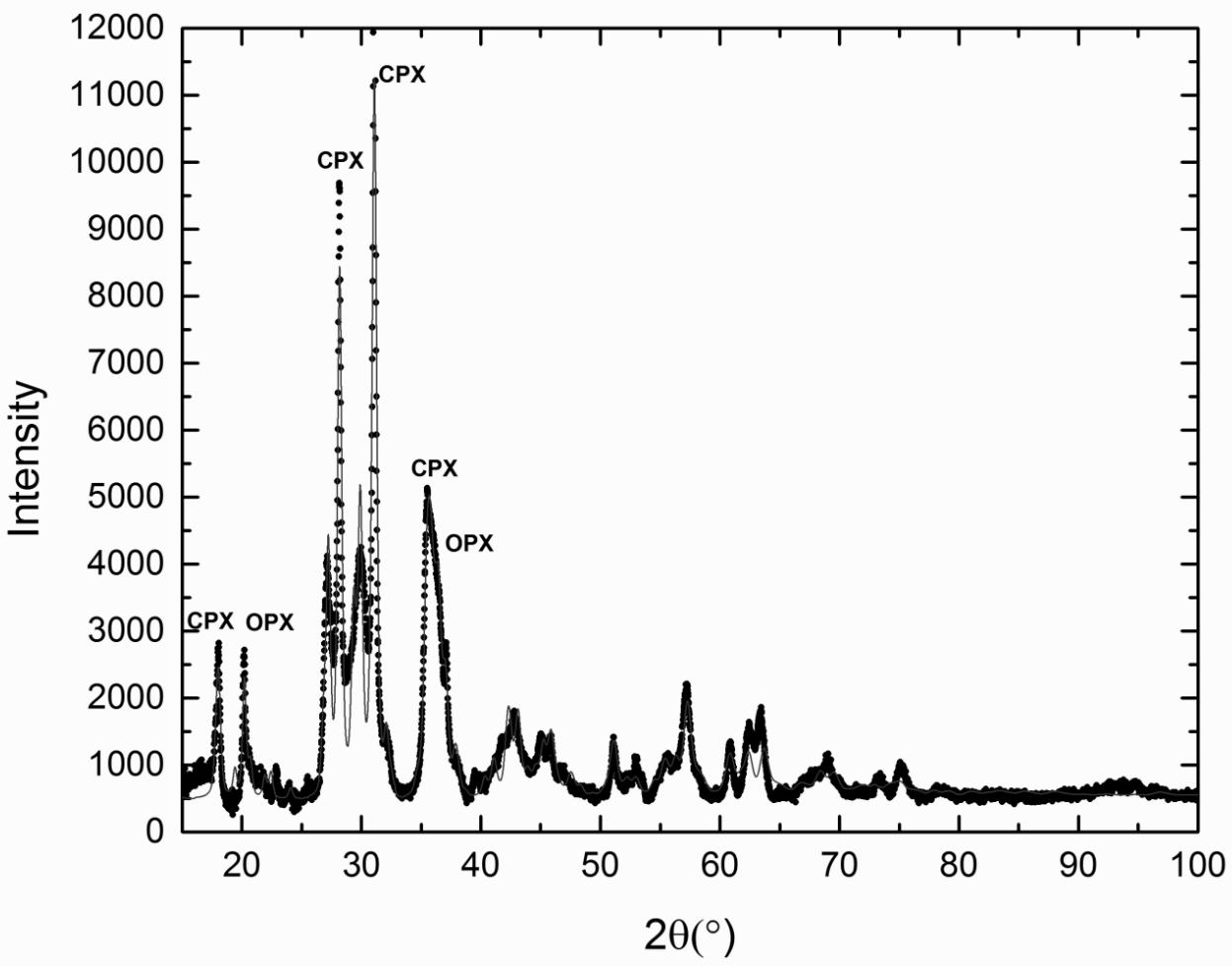

Figure 2: X-ray diffraction pattern for synthetic enstatite. Cpx = peaks for clinoenstatite, Opx = peaks for orthoenstatite.

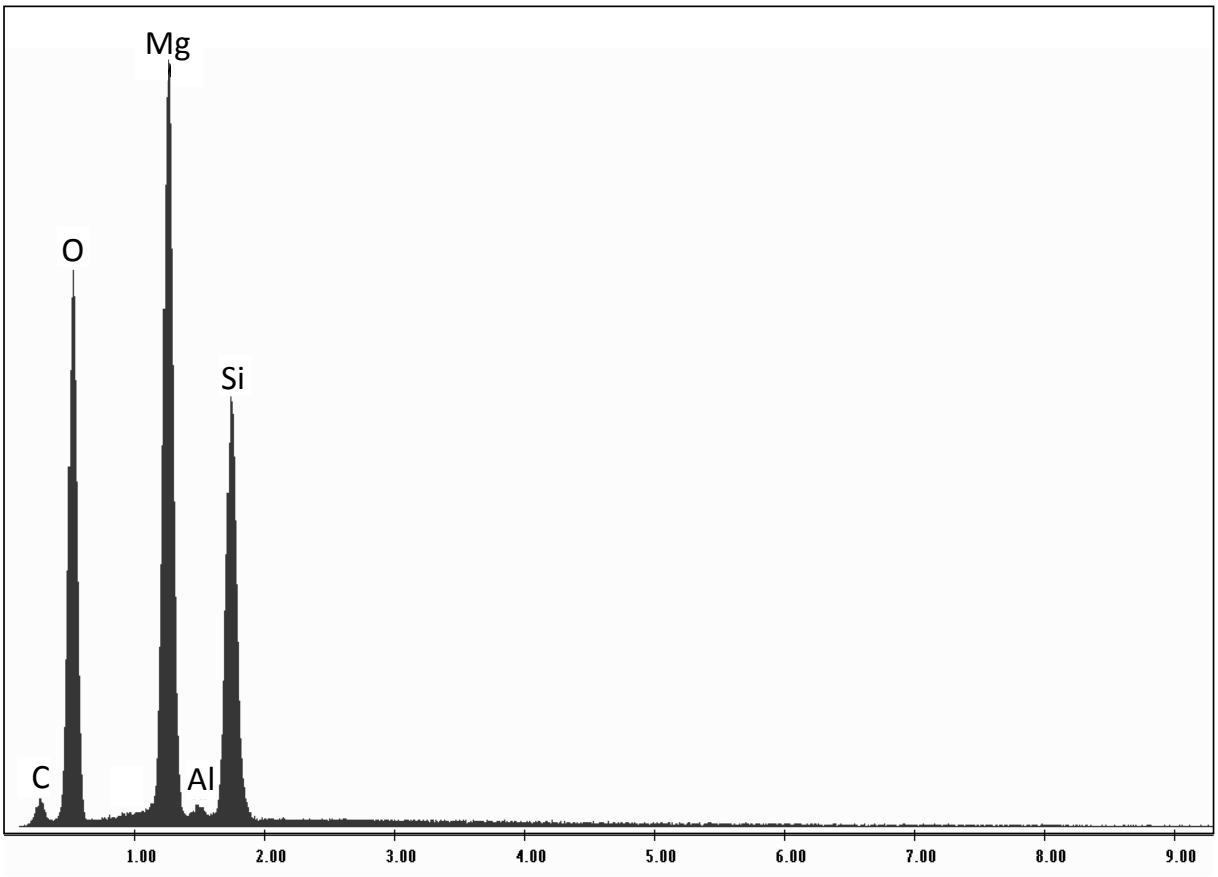

Figure 3: Energy dispersive spectrum of synthetic forsterite (batch 9). Carbon and aluminum peaks are from the sample mount.

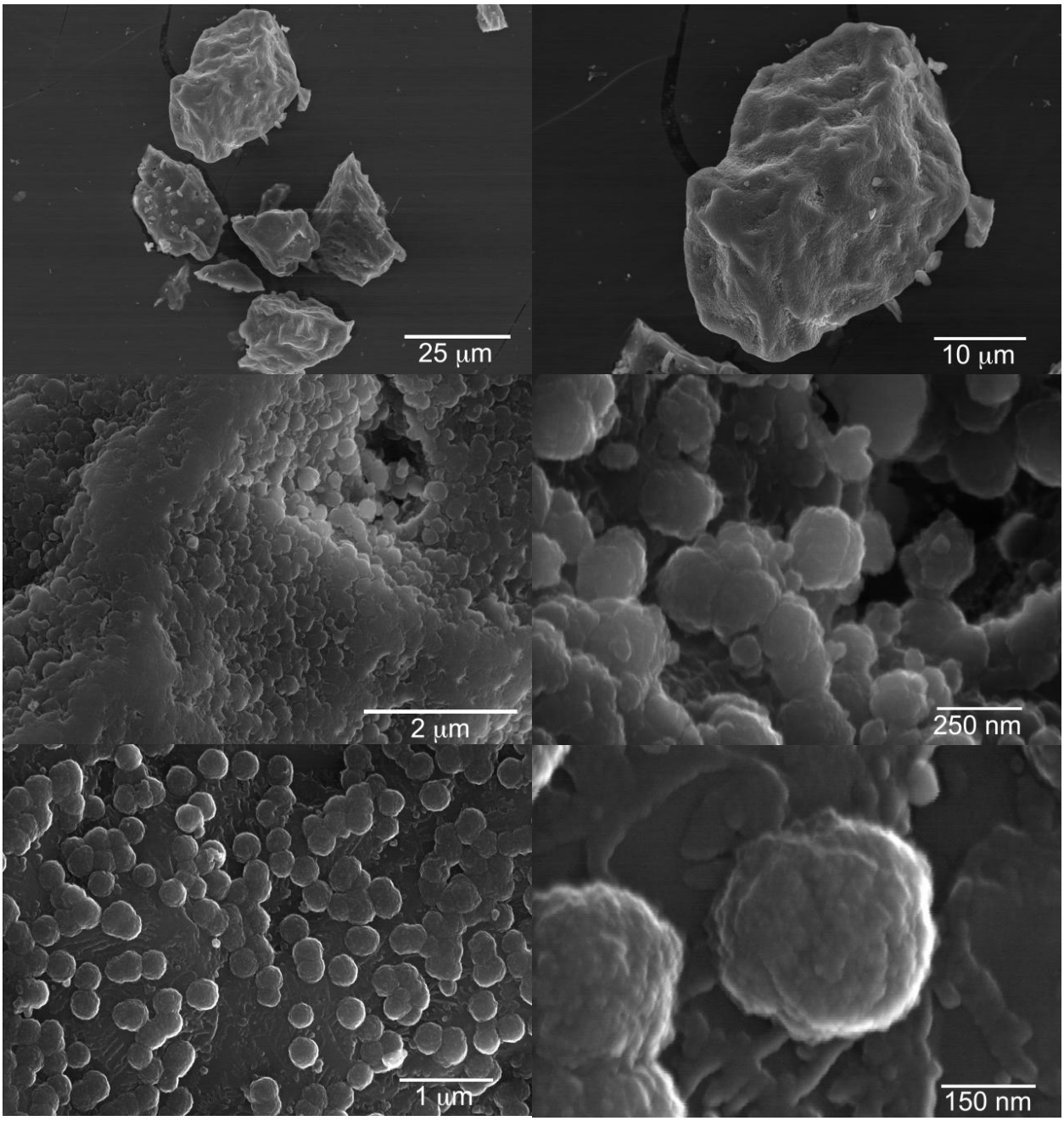

Figure 4: SEM images of synthetic forsterite (batch 9).

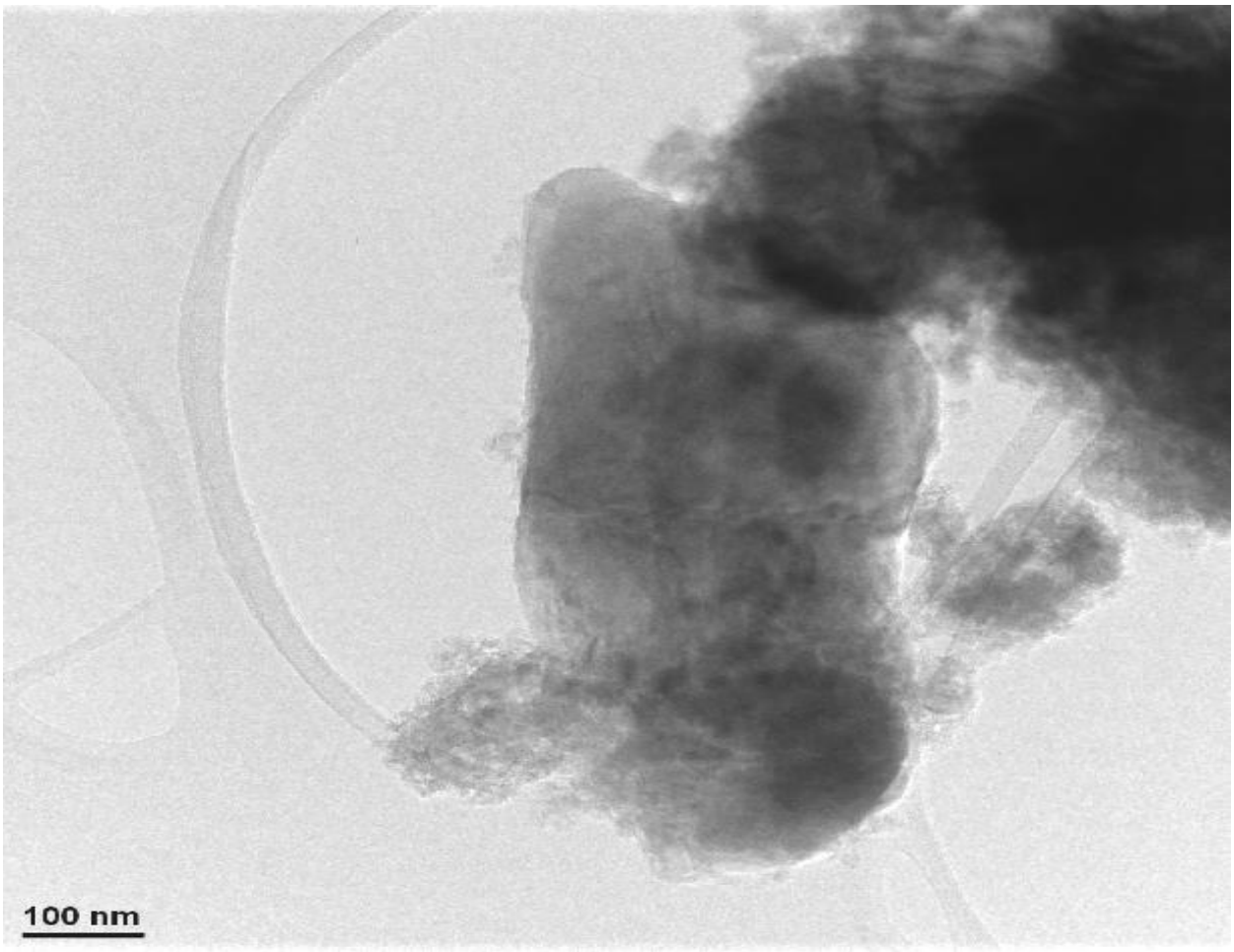

Figure 5: TEM image of synthetic forsterite. Remnants of the organic surfactant are apparent.

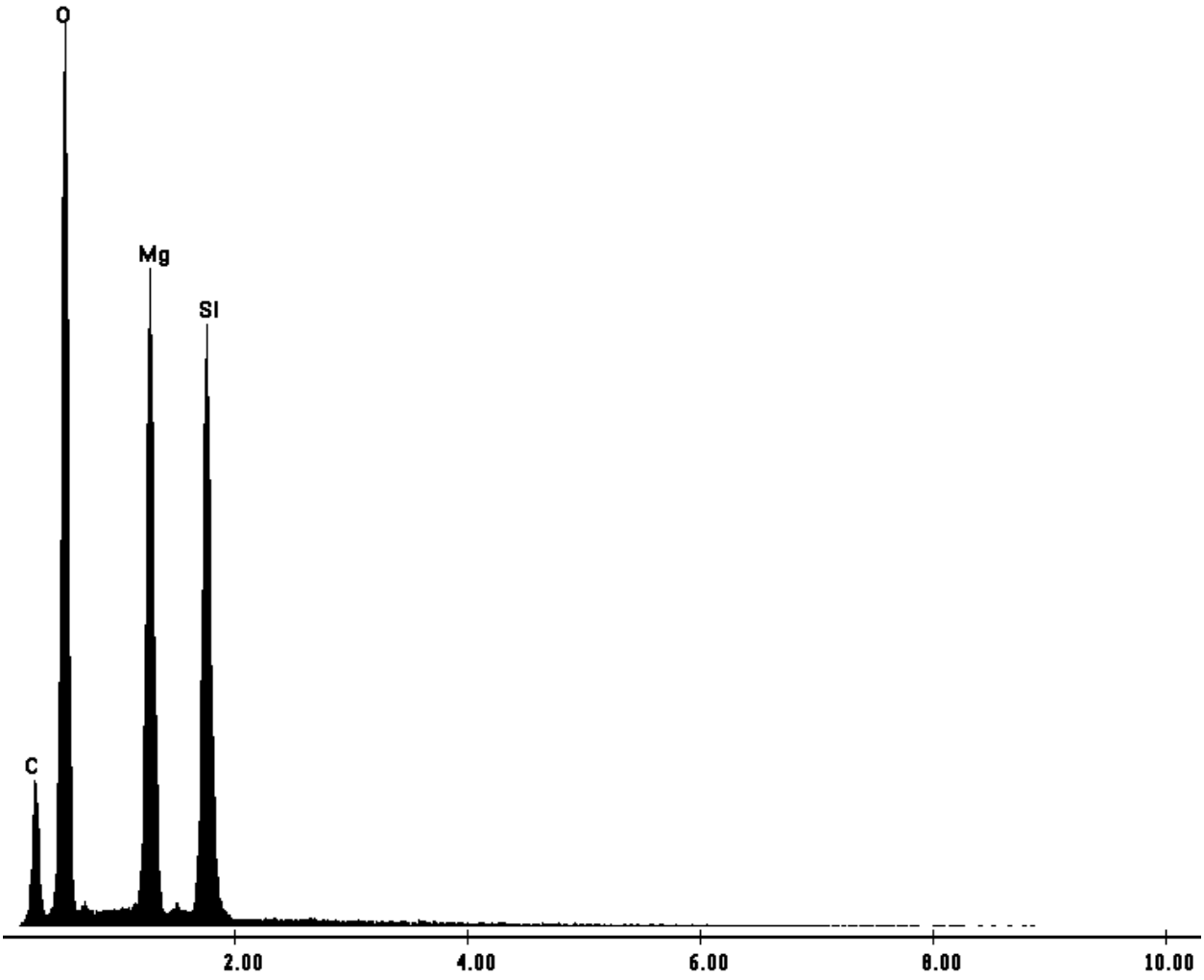

Figure 6. Energy dispersive spectrum of synthetic enstatite (batch 1). Carbon peak is from the sample mount and residual organic surfactant.

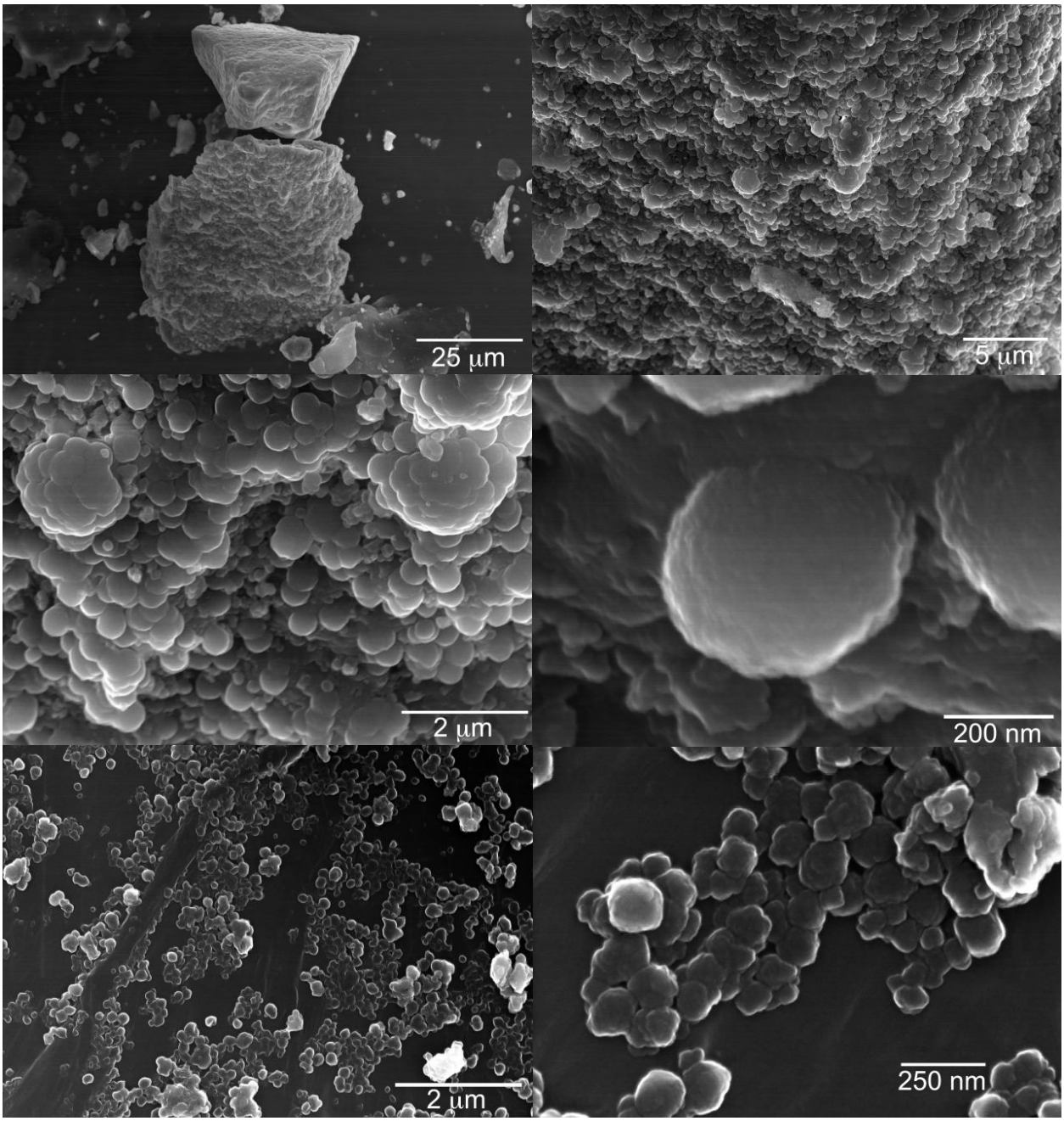

Figure 7: SEM images of synthetic enstatite (batch 1). The lower two images show enstatite utilizing residual organic surfactant as a growth substrate.

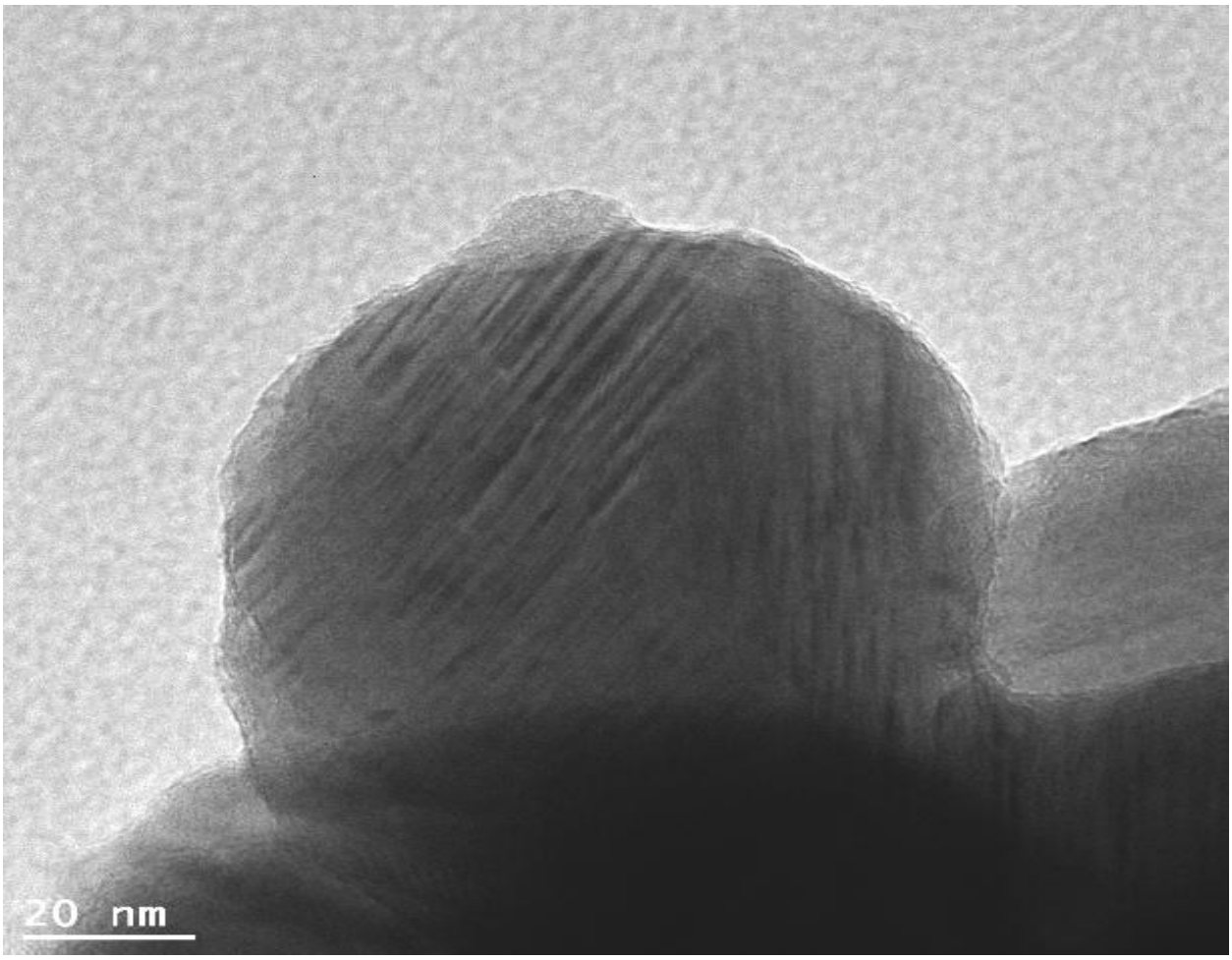

Figure 8: TEM image of synthetic enstatite. Minor remnants of the organic surfactant are apparent.

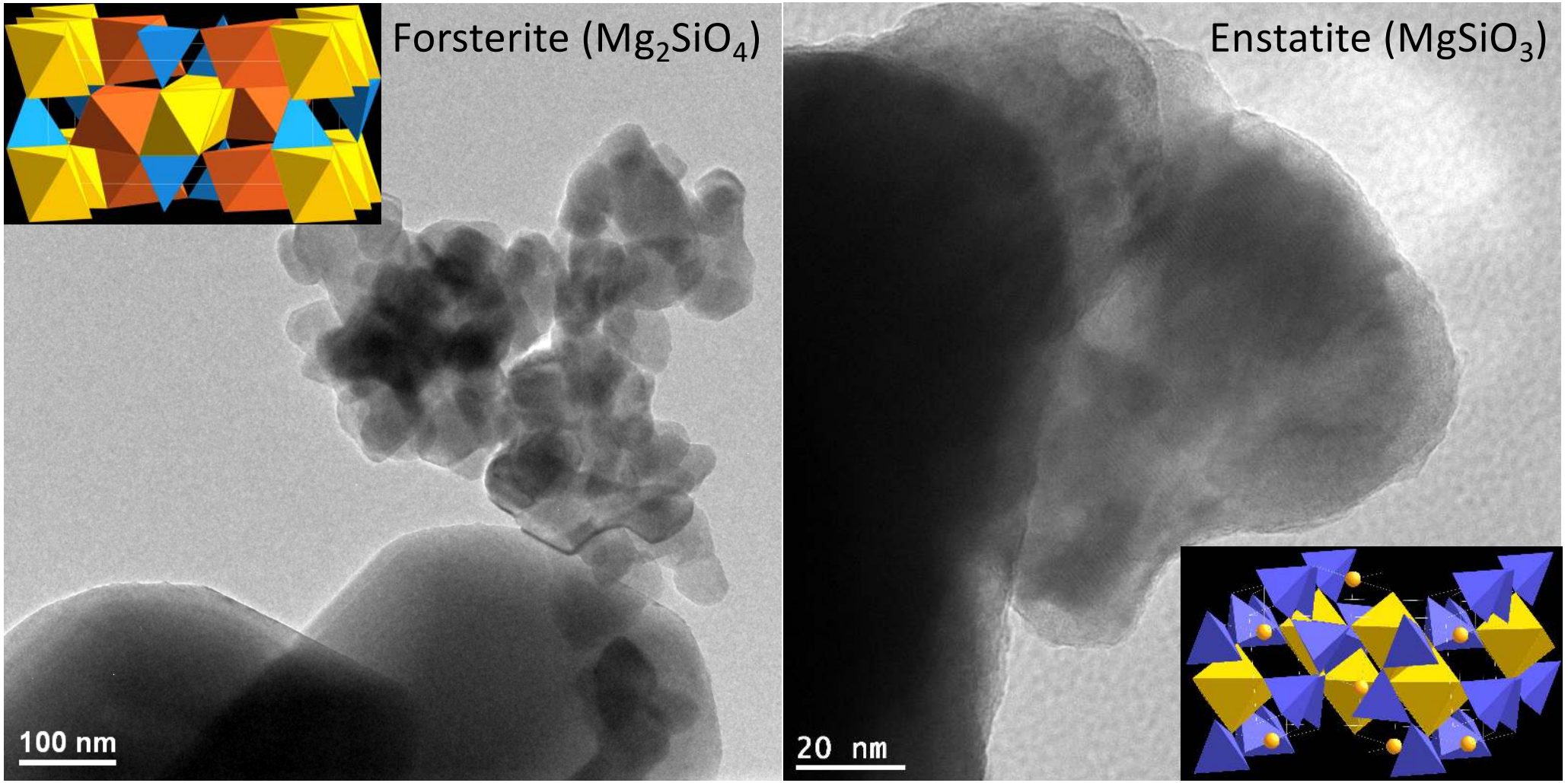
Forsterite (Mg_2SiO_4)
100 nm
Enstatite ($MgSiO_3$)
20 nm